

High-field pulsed electron–electron double resonance spectroscopy to determine the orientation of the tyrosyl radicals in ribonucleotide reductase

V. P. Denysenkov*, T. F. Prisner*, J. Stubbe^{†‡}, and M. Bennati^{*‡}

*Institute for Physical and Theoretical Chemistry and Center for Biomolecular Magnetic Resonance, J. W. Goethe University, 60438 Frankfurt am Main, Germany; and [†]Departments of Chemistry and Biology, Massachusetts Institute of Technology, Cambridge, MA 02139

Contributed by J. Stubbe, July 14, 2006

Class I ribonucleotide reductases (RNRs) are composed of two subunits, R1 and R2. The R2 subunit contains the essential diferric cluster-tyrosyl radical (Y·) cofactor, and R1 is the site of the conversion of nucleoside diphosphates to 2'-deoxynucleoside diphosphates. It has been proposed that the function of the tyrosyl radical in R2 is to generate a transient thiyl radical (C439·) in R1 over a distance of 35 Å, which in turn initiates the reduction process. EPR distance measurements provide a tool with which to study the mechanism of radical initiation in class I RNRs. These types of experiments at low magnetic fields and frequencies (0.3 T, 9 GHz) give insight into interradsical distances and populations. We present a pulsed electron–electron double resonance (PELDOR) experiment at high EPR frequency (180-GHz electron Larmor frequency) that detects the dipolar interaction between the Y·s in each protomer of RNR R2 from *Escherichia coli*. We observe a correlation between the orientation-dependent dipolar interaction and their resolved g-tensors. This information has allowed us to define the relative orientation of two radicals embedded in the active homodimeric protein in solution. This experiment demonstrates that high-field PELDOR spectroscopy is a powerful tool with which to study the assembly of proteins that contain multiple paramagnetic centers.

double electron–electron resonance | distance measurements

Ribonucleotide reductases (RNRs) catalyze the conversion of nucleotides to deoxynucleotides in all organisms. Class I RNR from *Escherichia coli* is composed of two homodimeric subunits (R1 and R2) that are thought to form a 1:1 complex (1). The R2 subunit contains the essential diferric cluster-tyrosyl radical (Y·) cofactor, and R1 is the site of the conversion of nucleoside diphosphates to 2'-deoxynucleoside diphosphates. The chemistry of nucleotide reduction is moderately well understood (2), and structures of R1 (3) and R2 (4, 5), as well as a recent structure of the R1:R2 holocomplex (6), are available. A major unresolved issue in this class of enzymes is the mechanism of radical initiation (7): How does the tyrosyl radical in R2 generate a transient thiyl radical in R1 over a distance of 35 Å? The current proposal for the radical propagation pathway is based on a docking model of R1 and R2 and involves aromatic amino acid residues (3, 8, 9). Evidence in support of the long distance and the docking model has been recently provided by pulsed EPR distance measurements (10). These experiments have detected the distance between the Y· in R2 and a nitrogen-centered radical in the active site of R1, providing structural information on the R1:R2 active complex in the presence of the substrate and the allosteric effector. The results provided the impetus to further explore the capability of the method at high magnetic fields.

The pulsed electron–electron double resonance (PELDOR) experiment detects weak dipolar interactions between radicals and is based on a two-frequency pulse sequence (11, 12). One frequency is required to select the detected radical spins, and the second one is required to perturb the coupled partner spin. The

perturbation causes a change in the dipolar field of the detected spin and results in a modulation of the time-domain spin echo signal as a function of the dipolar frequency. At low EPR frequencies (X band), this method has been successfully applied in structural biology to measure distances between native cofactors in proteins, such as those of photosystem II (13), hydrogenase (14), RNR (10, 15, 16), sulfhydryl oxidases (17), and pyruvate ferredoxin oxidoreductase (18) or, by using nitroxide spin labels, to determine distances in RNA (19), DNA (20), and membrane proteins (21, 22). A very early study by Larsen and Singel (23) investigated the effect of orientation dependence in PELDOR at low fields using nitroxide spin labels. Although the entire dipolar powder pattern was observed at all excitation positions in the EPR line, the relative amplitude of the dipolar spectral features varied across the EPR line, and the effect was analyzed to give orientational information.

At high frequencies, EPR spectra are dominated by the anisotropy of the g-tensors, and it is expected that the PELDOR modulation will become a complex function of the orientation of the dipolar tensor with respect to the molecular axes of the radicals. This information should permit the determination of an additional structural feature, the mutual orientation of the two interacting radicals (24). However, difficulties inherent with the experimental conditions at high fields and frequencies, such as the very small excitation bandwidth of the pulses combined with the large width of the EPR lines, has prevented so far the application of this method.

Here, we report a 180-GHz PELDOR experiment that detects the dipolar coupling between the Y·s in the R2 subunit of RNR from *E. coli*. The modulation signal is strongly correlated to the g-tensor of the excited radicals, and the pattern generated after excitation across the EPR line reveals direct information about the mutual orientation of the two radicals embedded in the protein. Particularly, under our experimental conditions, the protein was active and in a well known redox state, which represents a considerable advantage compared with x-ray structural investigations in single crystals. Our work demonstrates that this method is a unique spectroscopic tool for determining the relative orientation of proteins in biologically active form in solution complexes when suitable paramagnetic probes can be site-specifically attached or are already present in the proteins of interest.

Results

180-GHz PELDOR Time Traces. Typical 180-GHz four-pulse double electron–electron resonance traces recorded at $g_y < B < g_z$ in the

Conflict of interest statement: No conflicts declared.

Abbreviations: PELDOR, pulsed electron–electron double resonance; RNR, ribonucleotide reductase.

[†]To whom correspondence may be addressed. E-mail: stubbe@mit.edu or bennati@chemie.uni-frankfurt.de.

© 2006 by The National Academy of Sciences of the USA

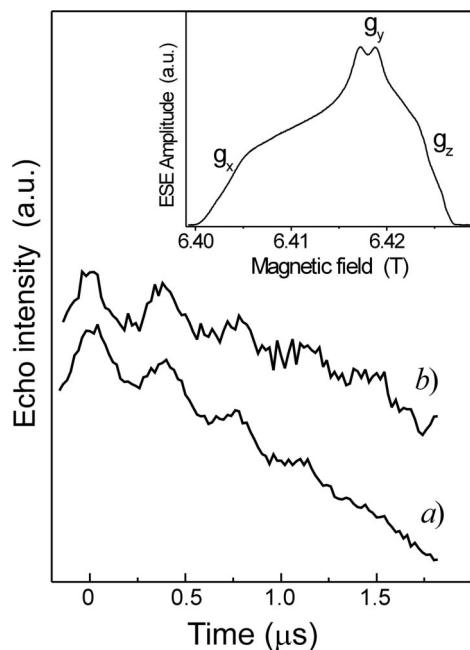


Fig. 1. Typical 180-GHz PELDOR traces of a 0.6 mM R2 protein solution (trace a) and of a 0.23 mM R2 protein solution (trace b) recorded at $g_y < B < g_z$. Both traces were normalized and plotted with an offset in the amplitude for comparison. The experimental conditions were as follows: $T = 5$ K, $t_r = 60$ ns (detection), $t_p = 80$ ns (pump), repetition time = 35 ms, 25 averages per point, five scans. (Inset) Echo-detected spectrum (180 GHz) of the tyrosyl radical in *E. coli* R2. The positions of the g values are marked.

EPR spectrum of R2 are displayed in Fig. 1. We observe a clear oscillation arising from a weak dipolar interaction and lasting over at least four modulation periods. The total acquisition time was 20 min for each trace. By comparing the trace of the sample with 0.6 mM $\beta 2$ (trace a) with the one with 0.23 mM (trace b), we note that the observed modulation depth remained approximately unchanged ($\lambda = 0.025 \pm 0.005$), whereas the S/N (defined here as percentage of the total echo at this time window), as well as the intrinsic echo decay, slightly decreased at lower concentration. Because no substantial advantages appeared from a dilution effect, we performed the orientation-selected study at the higher protein concentration.

Orientation-Selected Experiments. Fig. 2 shows the PELDOR modulation traces after subtraction of the echo decay recorded across the EPR line from $B \parallel g_z$ to $B \parallel g_x$. In the stack plot, the amplitudes were scaled as explained in *Materials and Methods* to account for the observed modulation depth. The traces show a clear field dependence in the modulation frequency as well as in the damping and in the modulation depth. A Fourier transformation of the data (not shown) indicated that the modulation frequency around $B \parallel g_z$ approaches the largest principal value of the dipolar tensor ($D_{\parallel} = 2.9$ MHz), whereas it reaches the perpendicular component at $B \parallel g_x$ ($D_{\perp} = 1.44$ MHz). This observation gives insight into the orientation of the radicals with respect to their interconnecting dipolar vector. Considering that the x axis of the g -tensor is located along the C–O bond of $Y\cdot$ and that the z axis is perpendicular to the ring plane [Fig. 3 (25, 26)], then the interconnecting dipolar vector is close to the direction normal to the plane of the tyrosine rings.

Spectral Analysis. A precise determination of the mutual orientation of the $Y\cdot$ s was achieved by analyzing the data with the model described in *Materials and Methods*. All principal values

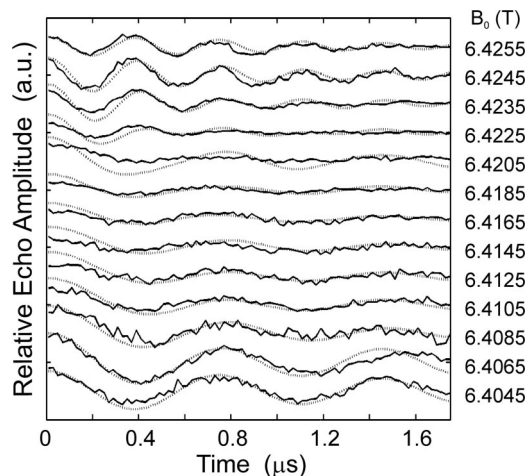


Fig. 2. Orientation-dependent PELDOR traces. Solid lines show orientation-dependent PELDOR traces recorded across the EPR line from $B \parallel g_z$ (top) to $B \parallel g_x$ (bottom). Dotted lines show the best global fit of the traces according to the model explained in *Materials and Methods*. The fit parameters are reported in Tables 1 and 2. The rmsd value amounted to 0.215.

of the g - and A -tensors are known from previous high-field EPR and electron nuclear double resonance experiments (26–28), and the principal axis values of the dipolar tensor were determined in the PELDOR measurements at X band (15). Because of the long distance (33 Å), the exchange interaction could be neglected (12). All of these values were kept fixed as reported in Table 1. As starting parameters for the fitting procedure, we used a set of three Euler angles (α, β, γ) for the rotation matrix R_d in Eq. 3, which we extracted from the x-ray structure of Högbom *et al.* (5). During the fit, these Euler angles were varied in steps of 0.1° . The effective field strength of the pump pulse was set to $\omega_1 = 4.0 \times 10^7$ rad/s; the field strength at the detection frequency was $\omega_1 = 5.2 \times 10^7$ rad/s according to a π pulse of 60 ns. These values correspond to spectral bandwidths of $\Delta B \approx 4.5$ G and $\Delta B \approx 6$ G, respectively, and are on the order of the inhomogeneous linewidth ($\Delta B_{\text{EPR}} \approx 6$ G) required in the simulation of the EPR powder pattern at 180 GHz. Thus, the orientation selection achieved at the edges of the EPR line is well in the “single-crystal-like” limit.

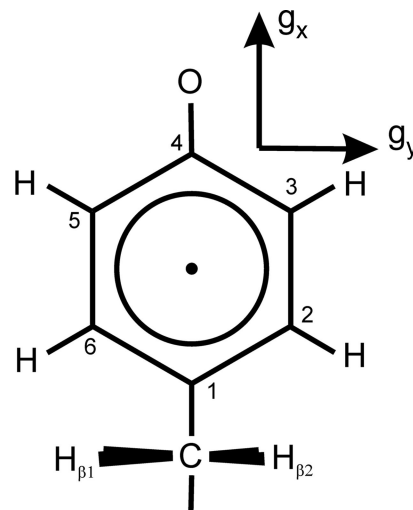


Fig. 3. Structure of the tyrosyl radical. The numbering of the carbon atoms and the directions of the g -tensor principal axes are collinear with the molecular axes (25, 26).

Table 1. Principal axis values of magnetic tensors for the Y• pair in the RNR R2 *E. coli* homodimer

Tensor	x	y	z	Ref.
g	2.00912	2.00457	2.00225	26
A_{H-β1}, G	20.7	19.8	18.7	26 and 27
A_{H-3,5}, G	-9.4	-2.9	-6.9	28 and 27
D, MHz	1.45	1.45	-2.9	15

Fig. 2 displays the global fit of the time traces obtained by this method. The resulting Euler angles of the matrix \mathbf{R}_d are summarized in Table 2. We note that the global fit succeeded in reproducing the orientation dependence of the dipolar frequencies, their damping, and their relative modulation amplitudes (λ_i/λ_{\max}). The most pronounced deviation is observed at the maximum of the EPR spectrum ($B = 6.4205$ T), where the calculated modulation depth slightly exceeds the experimental one. We suggest that this deviation is associated with spectral diffusion within the pumping hole, which is not considered in our simple model. The largest relative modulation depth was obtained at $B = 6.4065$ T (Fig. 2, second trace from the bottom), well in agreement with the experiment.[§]

The sensitivity of the method becomes more evident when comparing our global fit with a calculation of the curves under the assumption that the mutual orientation of the reduced Y122s in the crystal structure is conserved for the Y•s in solution (Fig. 4). These parameters for the matrices \mathbf{R}_d and $\mathbf{R}_{g(2) \rightarrow g(1)}$ are reported in Table 2. From the PELDOR results, it is clear that, at some field positions, in particular across the center of the EPR spectrum, this simulation deviates from the experimental data. The dipolar frequencies, and also their damping and their relative modulation amplitudes, are less well reproduced.

Discussion

We had previously reported that EPR distance measurements between endogenous radicals in class I RNRs represent a powerful tool with which to study the assembly of the protein subunits R1 and R2 and provide insight into the mechanism of radical initiation (10, 29). Nevertheless, distances, as well as information about radical distributions and orientations, are required to address issues about the enzymatic mechanism.

To demonstrate the feasibility of extracting radical orientations from PELDOR experiments at high fields, we improved our 180-GHz spectrometer to achieve $\pi/2$ detection pulses of 30 ns and loaded cavity quality factors of $\approx 1,000$. The gain in excitation bandwidth and spin sensitivity allowed us to apply the four-pulse, dead-time free double electron–electron resonance sequence, which permits reliable measurements of the full spectral contributions to the dipolar tensor and the determination of the absolute modulation depth. Typical dead-time free modulation traces as displayed in Figs. 1 and 2 could be readily obtained after acquisition times of minutes. The ability to observe small modulation effects ($\leq 6\%$) with large signal-to-noise ratios turned out to be an advantage of the high-field experiment. First, the relaxation times of an isolated radical at high fields are intrinsically longer than at lower fields (30). For the Y•s in RNR R2, this effect had already been reported in the T_1 spin lattice relaxation at 140 GHz (31). For the T_2 time at our experimental temperature ($T = 5$ K), we have measured an increase of a factor of two as compared with 9 GHz. The gain of spin echo intensity at the time point of detection, due to the long

[§]The calculated modulation depth does not take into account the fact that only a fraction of the radicals are paired, because this value is unknown. Also, relaxation effects are neglected. With these simplifications, the calculated absolute λ values exceed the experimental ones by a factor of two.

Table 2. Angles of rotation matrices for the Y• pair in the RNR R2 *E. coli* homodimer

Rotation	α	β	γ	Ref.
R_d	-79.1	32.1	75.6	This work
	-71.6	35.2	82.5	5
R_{g(2)→g(1)}[†]	83.7°	118.0°	95.7°	This work
	97.6°	106.2°	77.6°	5
$\varphi(g_i/Y122)$ [‡]	14°	13°	5°	This work
	10°	8°	5°	5

[†]Rotation matrix between the principal axes of the **g**-tensors of spin 1 and spin 2. The angles are Euler angles defined in a left-handed coordinate system for counterclockwise rotations.

[‡]Angles between the corresponding *x*, *y*, and *z* axes (g_i) of the **g**-tensor of Y• and the respective molecular axes of reduced Y122 from the x-ray structure of ref. 5.

T_2 , directly correlates with a gain in signal-to-noise ratio in the PELDOR trace. Secondly, orientation selection attenuates spectral damping in the modulation traces and thus enhances the sensitivity. This effect is evident when comparing traces recorded in the center of the EPR spectrum, where the largest density of spectral components contributes, with traces recorded at the edges of the spectrum (i.e., $B \parallel g_x$ and $B \parallel g_z$), where orientation selection is most efficient. In particular, we note that, at $B \parallel g_y$, the modulation disappears after the first oscillation, whereas at $B \parallel g_x$, almost no damping is observed.

The analysis of the orientation-dependent modulation traces requires the knowledge of all relevant magnetic parameters of the radicals, as well as an initial model for their orientation, to provide the input parameters in the fitting procedure. The well characterized Y•s in R2 from *E. coli* was chosen for this feasibility study because all of the magnetic parameters and an x-ray structure are available. Nevertheless, our results show that the method can be generally applied to any kind of biradical system, because the magnetic parameters can be determined independently in low- and high-field EPR experiments, and initial insight into their relative orientations can be extracted from inspection of the orientation-dependent traces if no other information is available.

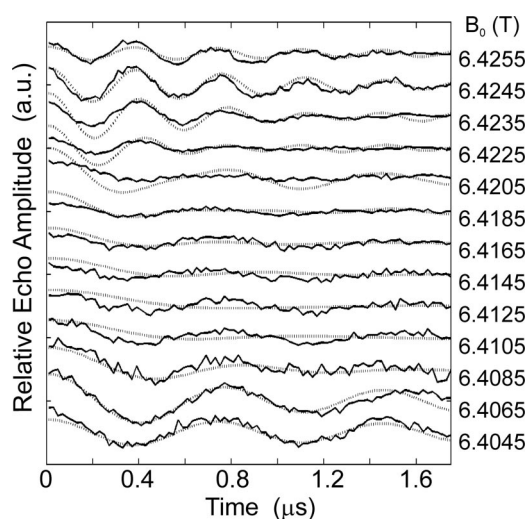


Fig. 4. Comparison of the experimental traces (solid lines) with a simulation of the curves (dotted lines) for a relative orientation of the radicals as given by the molecular axes of the reduced tyrosines in the crystal structure. The simulation parameters are given in Tables 1 and 2. The rmsd value amounted to 0.285.

The calculation was greatly simplified by inferring that the C_2 symmetric structure of the protein in the crystal is conserved in solution. For this case, only one transformation matrix was required to correlate the \mathbf{g} -tensors with the dipolar tensor, whereas the more general case necessitates two. The model was first justified by the observation that the distance between the radicals in frozen solution, 33.1 Å from X band PELDOR experiments, is consistent with the distance calculated from the center of gravity of the spin density distributions (32.6 Å) if the Y's are oriented like the reduced tyrosines in the crystal structure. The results indicate that the structures in solution and in the crystal are very similar. Our analysis provided a solution that is consistent with a dimeric structure of the protein and with only small deviations from the x-ray structure.

The results were summarized in terms of a displacement φ ($g_i/Y122$) of the observed \mathbf{g} -tensor axes with respect to the molecular axes in the crystal (Table 2). The displacement was calculated from the knowledge of the rotation matrix \mathbf{R}_d between the principal axis of the dipolar tensor and the \mathbf{g} -tensor and inferring that the direction of the dipolar vector in solution coincides with the one in the crystal. In Table 2, we compare displacements φ ($g_i/Y122$) of the three \mathbf{g} -tensor principal axes obtained with the ones reported from EPR measurements of the \mathbf{g} -tensor in single crystals at 94 GHz (5). Both methods revealed a small deviation in the orientation of $Y\cdot$ with respect to the reduced Y122 in the crystal structure. The agreement between the two independent results from the very different EPR methods is within 5° , with a consistent trend for the x , y , and z axes. This result is remarkable and provides strong support to our analysis. The differences of $\leq 5^\circ$ might give an estimate of the error or reflect an effect of the different matrices under study [frozen solution in this work versus crystal in Högbom *et al.* (5)].

In conclusion, our work has demonstrated the feasibility of nanometer distance measurements at high magnetic fields, the systematic observation of orientation dependence in the modulation time traces, and the feasibility of the spectral analysis that permits determination of additional structural information (i.e., the relative orientation of two radicals in frozen solution). The sample investigated, the R2 subunit of *E. coli* RNR, turned out to be an ideal candidate for this feasibility study, because the two interacting spin species were symmetry-related and had a well defined geometry with a unique relative orientation. In view of a more general applicability of the method, in particular with protein spin labeling experiments using [1-oxo-2,2,5,5-tetramethyl-pyrroline-3-methyl]-methanethiosulfonate or maleimide labels, the analysis might pose much greater challenges. Nevertheless, this technique has great potential for accessing structural information about protein-protein interactions and conformational changes when rigid paramagnetic species can be placed site-specifically into the protein of interest.

Materials and Methods

R2 protein from *E. coli* (specific activity of 7,550 nmol·mg⁻¹·min⁻¹) was grown and purified as described in ref. 32. The concentration was measured by using $\epsilon_{280} = 130,500$ M⁻¹·cm⁻¹. The radical concentration of 1.07 radicals per R2 (β_2) was determined by using the previously established drop-line correction method (33) and by 9-GHz continuous-wave EPR by using a 1 mM Cu²⁺ standard (34, 35). A value of 3.18 Fe per R2 was determined by using the ferrozine assay (36, 37). EPR tubes for 180-GHz spectroscopy (silica, o.d. of 0.55 mm, i.d. of 0.4 mm) were purchased from Spintec (Biebesheim, Germany).

180-GHz PELDOR Spectroscopy. PELDOR was performed with a home-built, 180-GHz pulsed EPR spectrometer extended for two-frequency irradiation (24, 38). For the pumping frequency, a mechanically tunable oscillator is adjusted to deliver frequencies in the range of 180 ± 2 GHz. The frequency of the pump and

detection pulses is monitored with an HP8563 spectrum analyzer, and a stability of ± 5 MHz can be achieved after ≈ 1 h of operation. A recently purchased 180-GHz frequency doubler (Virginia Diodes, Charlottesville, VA) allows for an output power of the microwave bridge of 50 mW. The available power, in combination with a cylindrical TE₀₁₁ cavity of $Q_{\text{load}} \approx 1,000$, translates into optimal $\pi/2$ pulse lengths of 30 ns at the observer frequency, which is tuned to the cavity resonance frequency. The pumping frequency was set 60 MHz away from the observer frequency, and this offset was kept constant during the whole experiment. The length of the pumping pulse was adjusted to ≈ 80 ns.

Dipolar modulation time traces were recorded with the four-pulse, dead-time free double electron-electron resonance sequence (39) by using a time window of 2 μ s between the second and third pulses and a pulse sequence repetition time of 35 ms at a temperature of 5 K. To obtain the orientation dependence of the modulation frequency, the resonant field position was varied through the EPR powder spectrum in steps of 20 G from $B \parallel g_x$ to $B \parallel g_y$ and in steps of 10 G from $B \parallel g_y$ to $B \parallel g_z$.

Analysis of Spectra. The intrinsic echo decay was eliminated from the modulation traces by fitting an exponential or a polynomial function to the traces and dividing the experimental data by the fitted function. The modulation depth λ was determined at each resonant field position by following the procedure described in ref. 12. Orientation-dependent stack plots were obtained after determining the relative amplitude $\lambda_i/\lambda_{\text{max}}$ of each trace (i) with respect to the trace with the largest modulation depth (λ_{max}) and scaling all normalized amplitudes with the corresponding factors $\lambda_i/\lambda_{\text{max}}$.

Time traces were analyzed with a home-written program in MATLAB that was implemented into a commercial fit routine, fitmincon, which is well suited for nonlinear problems, from the MATLAB toolbox. The best fit was obtained by calculating the rmsd between experiment and calculation from all points of the array of the traces and minimizing this function. The angular dependent resonance field positions for spin 1 and spin 2 of the $Y\cdot$ biradical were calculated in the high-field approximation by using the available hyperfine tensors of the strongly coupled protons (the β_1 and 3,5-ring protons; Fig. 3). The expression for the EPR resonances is described in Eq. 1,

$$h\nu = B\mu_B g(\theta, \varphi) + m_s a(\theta, \varphi), \quad [1]$$

where B is the magnetic field at detection, μ_B is the Bohr magneton, m_s is the electronic spin manifold, and g and a are the orientation-dependent g and hyperfine constants. In the high-field approximation, only the z components of the electron and nuclear spin operators, S_z and I_z , are taken into account, and g and a are given, respectively, by the g_{zz} and A_{zz} components of the dipolar and hyperfine tensors, expressed through appropriate transformations into the laboratory frame. These transformations for the detected spin (denoted as "1") and the pumped spin (denoted as "2") were introduced as following

$$\tilde{g}(1) = \mathbf{R}(\theta, \varphi) \mathbf{g}(1) \mathbf{R}^T(\theta, \varphi) \quad [2]$$

$$\tilde{g}(2) = \mathbf{R}(\theta, \varphi) [\mathbf{R}_d \mathbf{R}_{C_2} \mathbf{R}_d^T] \mathbf{g}(2) [\mathbf{R}_d \mathbf{R}_{C_2} \mathbf{R}_d^T]^T \mathbf{R}^T(\theta, \varphi). \quad [3]$$

Here, \tilde{g} denotes the \mathbf{g} -tensor in the laboratory frame; \mathbf{R} and \mathbf{R}^T are Euler rotation matrices and their transpositions. $\mathbf{R}(\theta, \varphi)$ describes the rotation from the \mathbf{g} (1)-tensor principal axis system to the laboratory frame; \mathbf{R}_d describes the rotation from the dipolar tensor principal axis system into the \mathbf{g} (1)-tensor. Assuming that the β_2 structure revealed in the crystal, with a C_2 axis perpendicular to the dipolar vector between the radicals, is preserved in solution, then a 180° rotation about this symmetry

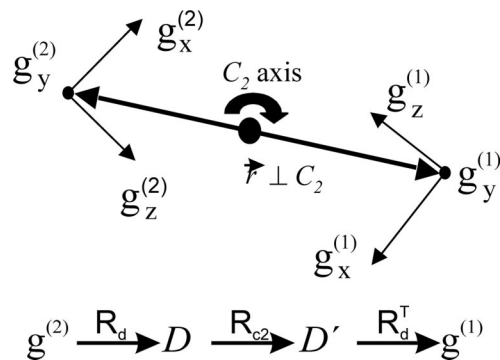


Fig. 5. Schematic transformation of the \mathbf{g} -tensor principal axes of spin 2 into the corresponding axes of spin 1 by means of the coordinate system of the dipolar tensor. The transformation takes advantage of the C_2 symmetry of the biradical.

axis (\mathbf{R}_{C_2}) transforms the \mathbf{g} -tensor principal axis system of spin 2 into the one of spin 1. With this assumption, the total transformation from $\mathbf{g}^{(1)}$ into $\mathbf{g}^{(2)}$ can be expressed by means of a “sandwich” transformation to the principal axis system of the dipolar tensor (see Eq. 3). Although the spin density on the radical is delocalized, the degree of spatial delocalization is small (28) compared with the biradical distance of 33 Å, and we

defined the direction of the z axis of the dipolar tensor as given by the vector interconnecting the center of gravity of spin density distribution. The y direction of the dipolar tensor was defined as coincident with the C_2 axis, leading to three Euler angles of \mathbf{R}_d as variables. This transformation is illustrated in Fig. 5. Similar transformations, as given in Eqs. 2 and 3, were also applied to all hyperfine tensors and to the dipolar tensor.

The PELDOR frequencies were calculated as a function of the selected orientations (θ, φ) at the detected and pumping fields of resonance. The angular orientations were selected by calculating the excitation profile of a 180° pulse according to ref. 40 and numerically collecting all angles that fall within this excitation range during the powder average. For simplicity, no additional inhomogeneous broadening function in the EPR spectrum was accounted in the angle selection. This procedure had been used in the past for the computation of orientation-selected electron nuclear double resonance spectra of tyrosyl radicals at similar fields (31, 41) and had led to satisfactory results. The modulation depth was computed as the fraction of spins belonging to a spin pair with respect to the total spectral intensity at the field of detection (24).

We thank J. Fritscher for donating MATLAB routines for computation of matrix transformations and for discussions. This work was supported by Deutsche Forschungsgemeinschaft Priority Programs 1051 (High-Field EPR in Physics, Chemistry, and Biology) and 1071 (Radicals in Enzymatic Catalysis).

- Jordan, A. & Reichard, P. (1998) *Annu. Rev. Biochem.* **67**, 71–98.
- Licht, S. & Stubbe, J. (1999) in *Comprehensive Natural Products Chemistry*, eds. Barton, S. D., Nakanishi, K., Meth-Cohn, O. & Poulter, C. D. (Elsevier Science, New York), Vol. 5, pp. 163.
- Uhlin, U. & Eklund, H. (1994) *Nature* **370**, 533–539.
- Nordlund, P., Sjöberg, B.-M. & Eklund, H. (1990) *Nature* **345**, 593–598.
- Högbom, M., Galander, M., Andersson, M., Kolberg, M., Hofbauer, W., Lassmann, G., Nordlund, P. & Lenzian, F. (2003) *Proc. Natl. Acad. Sci. USA* **100**, 3209–3214.
- Uppsten, M., Färnegårdh, M., Domkin, V. & Uhlin, U. (2006) *J. Mol. Biol.* **359**, 365–377.
- Stubbe, J., Nocera, D. G., Yee, C. S. & Chang, M. C. Y. (2003) *Chem. Rev.* **103**, 2167.
- Seyedsayamdost, M. R. & Stubbe, J. (2006) *J. Am. Chem. Soc.* **128**, 2522–2523.
- Seyedsayamdost, M. R., Yee, C. S., Reece, S. Y., Nocera, D. G. & Stubbe, J. (2006) *J. Am. Chem. Soc.* **128**, 1562–1568.
- Bennati, M., Robblee, J., Mugnaini, V., Stubbe, J., Freed, J. H. & Borbat, P. P. (2005) *J. Am. Chem. Soc.* **127**, 15014–15015.
- Milov, A. D., Ponomarev, A. B. & Tsvetkov, Y. D. (1984) *Chem. Phys. Lett.* **110**, 67–72.
- Jeschke, G. (2002) *Macromol. Rapid Commun.* **23**, 227–246.
- Hara, H., Kawamori, A., Astashkin, A. V. & Ono, T. (1996) *Biochim. Biophys. Acta* **1276**, 140–146.
- Elsässer, C., Brecht, M. & Bittl, R. (2002) *J. Am. Chem. Soc.* **124**, 12606–12611.
- Bennati, M., Weber, A., Antonic, J., Perlstein, D. L., Robblee, J. & Stubbe, J. (2003) *J. Am. Chem. Soc.* **125**, 14988.
- Biglino, D., Schmidt, P. P., Reijerse, E. J. & Lubitz, W. (2006) *Phys. Chem. Chem. Phys.* **8**, 58–62.
- Kay, C. W. M., Elsässer, C., Bittl, R., Farrell, S. R. & Thorpe, C. (2006) *J. Am. Chem. Soc.* **128**, 76–77.
- Astashkin, A. V., Seravalli, J., Mansoorabadi, S. O., Reed, G. H. & Ragsdale, S. W. (2006) *J. Am. Chem. Soc.* **128**, 3888–3889.
- Schiemann, O., Weber, A., Edwards, T. E., Prisner, T. F. & Sigurdsson, S. T. (2003) *J. Am. Chem. Soc.* **125**, 3434–3435.
- Schiemann, O., Piton, N., Mu, Y., Stock, G., Engels, J. W. & Prisner, T. F. (2004) *J. Am. Chem. Soc.* **126**, 5722–5729.
- Hilger, D., Jung, H., Padan, E., Wegener, C., Vogel, K.-P., Steinhoff, H.-J. & Jeschke, G. (2005) *Biophys. J.* **89**, 1328–1338.
- Banham, J. E., Timmel, C. R., Abbott, R. J. M., Lea, S. M. & Jeschke, G. (2006) *Angew. Chem. Int. Ed.* **45**, 1058–1061.
- Larsen, R. G. & Singel, D. J. (1993) *J. Chem. Phys.* **98**, 5134–5146.
- Denysenkov, V. P., Prisner, T. F., Stubbe, J. & Bennati, M. (2005) *Appl. Magn. Reson.* **29**, 375–384.
- Fasanella, E. L. & Gordy, W. (1969) *Proc. Natl. Acad. Sci. USA* **62**, 299–304.
- Gerfen, G. J., Bellew, B. F., Un, S., Bollinger, J. M., Jr., Stubbe, J., Griffin, R. G. & Singel, D. J. (1993) *J. Am. Chem. Soc.* **115**, 6420–6421.
- Bender, C. J., Sahlin, M., Babcock, G. T., Barry, B. A., Chandrashekar, T. K., Salowe, S. P., Stubbe, J., Lindström, B., Petersson, L., Ehrenberg, A. & Sjöberg, B.-M. (1989) *J. Am. Chem. Soc.* **111**, 8076–8083.
- Honganson, C. W., Sahlin, M., Sjöberg, B.-M. & Babcock, G. T. (1996) *J. Am. Chem. Soc.* **118**, 4672–4679.
- Bennati, M., Lenzian, F., Schmittel, M. & Zipse, H. (2005) *Biol. Chem.* **386**, 1007–1022.
- Prisner, T. F. (1997) *Adv. Magn. Opt. Reson.* **20**, 245–299.
- Bar, G., Bennati, M., Nguyen, H.-H. T., Ge, J., Stubbe, J. & Griffin, R. G. (2001) *J. Am. Chem. Soc.* **123**, 3569–3576.
- Salowe, S. P. & Stubbe, J. (1986) *J. Bacteriol.* **165**, 363–366.
- Bollinger, J. M., Jr., Edmondson, D. E., Huynh, B. H., Filley, J., Norton, J. R. & Stubbe, J. (1991) *Science* **253**, 292–298.
- Malmström, B. G., Reinhammar, B. & Vänngård, T. (1970) *Biochim. Biophys. Acta* **205**, 48–57.
- Aasa, R. & Vänngård, T. (1975) *J. Magn. Reson.* **19**, 308–315.
- Massey, V. (1957) *J. Biol. Chem.* **229**, 763–770.
- Stokey, L. L. (1970) *J. Biol. Chem.* **245**, 779–781.
- Hertel, M. M., Denysenkov, V. P., Bennati, M. & Prisner, T. F. (2005) *Magn. Reson. Chem.* **43**, 248–255.
- Pannier, M., Veit, S., Godt, A., Jeschke, G. & Spiess, H. W. (2000) *J. Magn. Reson.* **142**, 331–340.
- Grupp, A. & Mehring, M. (1990) in *Modern Pulsed and CW Electron Spin Resonance*, eds. Kevan, L. & Bowman, M. (Wiley, New York), p. 195.
- Bennati, M., Farrar, C. T., Bryant, J. A., Inati, S. J., Weis, V., Gerfen, G. J., Riggs-Gelasco, P., Stubbe, J. & Griffin, R. G. (1999) *J. Magn. Reson.* **138**, 232–243.